Reinforced concrete columns exposed to standard fire: Comparison among different constitutive models for concrete at high temperature

P. Bamonte *, F. Lo Monte

Department of Civil and Environmental Engineering, Politecnico di Milano, Piazza Leonardo da Vinci 32, 20133 Milan, Italy

Received 30 May 2014
Received in revised form 14 October 2014
Accepted 23 November 2014

1. Introduction

Since the early studies on heat-exposed concrete in the past century, reinforced concrete (R/C) structures showed good performance in fire thanks to some typical features of cement-based materials such as incombustibility and low thermal diffusivity.This latter property allows the external heat-damaged layers to protect the inner core from attaining too high temperature, even in the case of long fire durations. On the other hand, however, concrete mechanical properties are significantly influenced by high temperature (mainly above 400–500 °C). In particular, deformability is affected by both the thermal damage and the presence of further components of the load-induced deformation, namely the time-dependant creep strain and the temperature-induced transient strain. These two latter contributions of deformation proved to be of primary importance in modelling concrete at high temperature [1–4], being the cause of both a reduction of concrete apparent stiffness, with the ensuing enhancement of second-order effects, and a relaxation of the thermal stresses. This is one of the reasons why axially-restrained heated specimens do not collapse because of the thermal stresses induced by restrained thermal dilation. Clearly, to accurately evaluate the structural behaviour of any given heat-exposed R/C member, all the aforementioned strain components must be suitably taken into account: in redundant structures, because deformations and displacements influence the internal forces; in slender columns subjected to an eccentric axial force [5], because of the role played by second-order effects.

Within this context, a few constitutive models have been proposed in the past, taking into account creep and transient strains both explicitly or implicitly (by defining a single total load-induced strain component, which lumps instantaneous load-induced strain, creep and transient strains). Among the different formulations proposed in the literature, the four models investigated in the present paper are those by Anderberg and Thelandersson [6], Khoury and Terro [7], Schneider et al. [8] as well as the stress–strain law included in Eurocode 2 – Fire Design (EC2) [9]. The former three models define explicit transient and creep strain components, while the latter is an implicit formulation.

The present study aims at numerically simulating a number of well-documented full-scale tests on R/C columns exposed to Standard Fire, with three main objectives: (a) to assess the relevance of critical issues such as creep and transient strains, and

* Corresponding author. Fax: +39 02 23994220.
E-mail address: patrick.bamonte@polimi.it (P. Bamonte).

second-order effects, (b) to verify the reliability of a Beam Finite Element analysis to numerically simulate the structural response of R/C members in fire, and (c) to make a systematic comparison among the abovementioned constitutive models. To this end, an ad hoc Beam Finite Element (FE) code has been developed by using a Fortran solver and GID as pre- and post-processor. A preliminary study on the same topics was already performed in 2010 [10]. It is worth underlining that, because of their typical loading conditions (prevailing axial force), columns are best-suited to highlight critical aspects related to concrete behaviour in compression.

Generally speaking, the simulation of heat-exposed R/C structures in fire would require the solution of an hygro-thermo-mechanical problem. If spalling is neglected, however, the hygral framework can be disregarded and only the thermo-mechanical problem can be dealt with. This can be performed by using either 3D FE [2,7,11] or 1D FE models [12–15]. In the present study, since spalling is not considered, the thermo-mechanical problem only is taken into account and a Beam FE code is preferred, because of the simplicity in implementing and the convenience for structural design (where a simple and time-saving approach is surely preferable). As a matter of fact, in the literature also simplified analytical models for the evaluation of the time to failure of slender R/C members have been proposed for simple loading and restraint conditions [16,17].

2. Concrete behaviour in compression during heating

2.1. Concrete kinematics in hot conditions

The kinematics of concrete during heating is characterized by the presence of four contributions, namely: thermal strain $\varepsilon_{th}(T)$, instantaneous stress-related strain $\varepsilon_{\sigma}(\sigma,T)$, transient strain $\varepsilon_{tr}(\sigma,T)$, and creep strain $\varepsilon_{cr}(\sigma,T,t)$. Hence, the load-induced strain $\varepsilon_{\sigma,tr,cr}(\sigma, T, t)$ is the sum of three contributions: $\varepsilon_{\sigma}(\sigma,T)$, $\varepsilon_{tr}(\sigma,T)$, and $\varepsilon_{cr}(\sigma,T,t)$.

The *thermal strain* ε_{th} represents the variation of the specific length induced by heating; it is a function of temperature only and is mainly influenced by the aggregate type. The thermal strain is usually measured on heat-exposed unstressed specimens.

The *instantaneous stress-related strain* ε_{σ} occurs instantaneously in heated concrete at a given temperature upon the application of an external load (= *instantaneous load-induced strain*). It is usually worked out by means of simple compression tests on specimens heated at a reference temperature T.

The *transient strain* ε_{tr} is an additional contribution to the strain induced by load and seems to be related mainly to the properties of the cement paste. As such, it could be reduced by increasing the quantity of aggregates [18]. The transient strain plays a very important role during heating, because it represents the largest contribution to the load-induced strain. The most important features of the transient strain include: (a) occurrence only during first heating [19]; (b) irreversibility; and (c) stress-, time- and temperature-dependency (though time-dependency becomes negligible for temperatures above 100 °C [1]). It is generally evaluated via compression tests performed on specimens heated up to collapse under a constant sustained level of stress σ.

The *creep strain* ε_{cr} has basically the same features of creep at ambient temperature, but with higher values, due to the effect on the rate of bond breakages of both temperature and water microdiffusion between capillary and gel pores [20]. It can be determined by means of compression tests on specimens heated to a reference temperature T and subjected to a given stress σ maintained for a time duration t.

As confirmed by experimental evidence [2], the principle of superposition can be assumed; then, the total strain ε_{tot} can be expressed by Eq.(1):

$$\varepsilon_{tot}(\sigma, T, t) = \varepsilon_{th}(T) + \varepsilon_{\sigma}(\sigma, T) + \varepsilon_{tr}(\sigma, T) + \varepsilon_{cr}(\sigma, T, t) \quad (1)$$

Both transient and creep strains bring in a significant increase of the load-induced strain, thus making concrete apparent stiffness lower: as already mentioned, this effect has both pros (lower sensitivity to restrained thermal dilation thanks to the relaxation of thermal stresses [4]) and cons (higher sensitivity to second-order effects [4,5]). Whether the former or the latter prevails is something that cannot be foretold, due to the several variables involved in the problem, such as geometry, structural layout, boundary restraints, etc. For common values of fire duration, however, the creep strain plays a minor role compared to the transient strain, and is often either neglected or lumped into the transient strain [21].

The models (that implicitly or explicitly include transient and creep phenomena) considered in this paper will be indicated as follows:

Model 1: Anderberg and Thelandersson's model [6];
Model 2: Khoury et al.'s model, developed at the beginning of the 80s, and later refined by Terro [7] for structural applications;
Model 3: Schneider, Schneider and Franssen's model [8];
Model 4: EC2's model [9].

The main features of the aforementioned models will be now briefly recalled.

2.1.1. Model 1: Anderberg and Thelandersson

Anderberg and Thelandersson [6] defined transient and creep strains separately, as expressed in Eqs. (2) and (3):

$$\varepsilon_{tr}(\sigma, T) = k_{tr}\frac{\sigma(\varepsilon_{\sigma})}{f_c^{20}}\varepsilon_{th} \quad (2)$$

$$\varepsilon_{cr}(\sigma, T, t) = 5.3\cdot10^{-4}\cdot\frac{\sigma(\varepsilon_{\sigma})}{f_c^{20}}\cdot\sqrt{\frac{t}{3}}e^{3.04\cdot10^{-3}\cdot(T-20)} \quad (3)$$

being k_{tr} a constant ranging from 1.80 to 2.35 for ordinary concrete, depending mostly on aggregate type (for siliceous aggregates the recommended value is k_{tr}=2.35), f_c^{20} the cylindrical compressive strength at 20 °C, f_c^{T} the cylindrical compressive strength at temperature T, and t the time expressed in hours.

It is worth noting that the transient strain depends on the temperature only, through the thermal strain ε_{th}. On the other hand, the creep strain depends on both time and temperature. Considering, however, that according to Eqs. (2) and (3) the creep strain attains significantly smaller values than the other strain components, generally, the dependency of the load-induced strain on time is limited.

2.1.2. Model 2: Khoury and Terro

Khoury introduced the concept of *load-induced thermal strain (LITS)* as the contribution to the load-induced strain caused by heating in addition to the purely elastic strain occurring at room temperature. LITS was evaluated starting from the analysis of several experimental results obtained at high temperature (up to 600 °C, [1,2,7]) and can be expressed by means of Eq. (4) [7]:

$$\mathrm{LITS}(\sigma, T) = \varepsilon_{\sigma}(\sigma, T) + \varepsilon_{tr}(\sigma, T) + \varepsilon_{cr}(\sigma, T) - \frac{\sigma}{E_0} = \varepsilon_{tot}(\sigma, T) - \varepsilon_{th}(T) - \frac{\sigma}{E_0} = \varepsilon_{\sigma,tr,cr}(\sigma, T) - \frac{\sigma}{E_0} \quad (4)$$

where E_0 is the initial tangent modulus of concrete in virgin conditions.

The instantaneous stress-related strain is then divided into two contributions: (a) purely elastic strain at room temperature, taken into account by σ/E_0, and (b) thermally-induced instantaneous stress-related strain caused by the decay of the elastic modulus with temperature, taken into account by LITS together with creep and transient strains.

LITS is defined as a function of stress and temperature, while time-dependency is neglected, as reported in Eqs. (5) and (6):

$$\mathrm{LITS}(0.3f_c^{20},T) = -(43.87 - 2.73T - 6.35\cdot10^{-2}T^2 + 2.19\cdot10^{-4}T^3 - 2.77\cdot10^{-7}T^4)\cdot10^{-6} \quad (5)$$

$$\mathrm{LITS}(\sigma, T) = \mathrm{LITS}\left(0.3f_c^{20}, T\right)\left(0.032 + 3.226\frac{\sigma}{f_c^{20}}\right) \quad (6)$$

Once the relation between stress and instantaneous stress-related strain ε_σ is defined (for instance by assuming the stress–strain diagram proposed by Schneider [22]), the expression of transient and creep strains, $\varepsilon_{tr,cr} = \varepsilon_{tr}+\varepsilon_{cr}$, can be obtained by subtracting the instantaneous stress-related strain ε_σ from $\varepsilon_{\sigma,tr,cr} = \mathrm{LITS}+\sigma/E_0$.

2.1.3. Model 3: Schneider, Schneider and Franssen

Schneider et al. [8] keep the recoverable component (elastic strain ε_{el}) separated from the irrecoverable – or partially irrecoverable – components (plastic, creep and transient strains); then the instantaneous stress-related strain is divided into an instantaneous elastic component ε_{el} and an instantaneous plastic component ε_{pl}, as expressed in Eqs. (7)–(10).

$$\varepsilon_{tot}(\sigma, T, t) = \varepsilon_{th}(T) + \varepsilon_{el}(\sigma, T) + \varepsilon_{pl}(\sigma, T) + \varepsilon_{tr}(\sigma, T) + \varepsilon_{cr}(\sigma, T, t) \quad (7)$$

$$\varepsilon_{el}(T,\ \alpha) = \frac{\sigma(t)}{E(T,\ \alpha)} \quad (8)$$

$$\varepsilon_{pl}(T,\ \alpha) = \kappa\frac{\sigma(t)}{E(T,\ \alpha)} \quad (9)$$

$$\varepsilon_{\sigma,tr,cr}(\sigma, T) = (1 + \varphi)\frac{\sigma(t)}{E(T)} \quad (10)$$

where $\alpha=\sigma(t)/f_c^{20}$ takes into account the influence of the load history, κ is a function (see [8]) and φ is the *transient creep function* defined via Eqs. (11) and (12):

$$\varphi = C_1\tanh\gamma_w(T - 20\ ^\circ\mathrm{C}) + C_2\tanh\gamma_0\left(T - T_g\right) + C_3 \quad (11)$$

$$\gamma_w = 0.3\cdot10^{-3}w^{0.5} + 2.2\cdot10^{-3} \le 2.8\cdot10^{-3} \quad (12)$$

being w the moisture content expressed in % by mass, and C_1, C_2, C_3, and T_g parameters that can be determined according to [8]. It is worth noting that the transient creep function does not depend on time.

The term $\varphi\ \sigma(t)/E(T)$ comprises plastic, transient and creep strains, and also part of the elastic contribution. The model takes into account the influence of the load history on the decay of concrete mechanical properties during heating through coefficient α. As shown in Eq. (10), however, the influence of the load history on the load-induced strain is negligible, according to the available experimental results [8].

The instantaneous stress-related strain ε_σ, taking into account both elastic and plastic contributions, is defined according to Schneider [22]; hence, the expression of transient and creep strains, $\varepsilon_{tr,cr}$, can be obtained by subtracting ε_σ from $\varepsilon_{\sigma,tr,cr}$.

2.1.4. Model 4: EC2

In order to simulate concrete mechanical response during heating, it is also possible to follow the approach suggested by EC2, in which the total strain is split into two components only (implicit formulation):

$$\varepsilon_{tot}(\sigma, T) = \varepsilon_{th}(T) + \varepsilon_{\sigma,tr,cr}(\sigma, T) \quad (13)$$

Obviously, the use of Eq. (13) requires $\varepsilon_{\sigma,tr,cr}$ to be properly defined in order to take into account all the strain components induced by the load, such as the instantaneous stress-related strain, the transient strain and the creep strain. On the other hand, this implicit formulation greatly simplifies the iteration procedure that is required in a non-linear numerical analysis.

2.2. Stress–strain relations

The relationship between stress and instantaneous stress-related strain, that is common to the models illustrated in the previous section, is generally described by means of the formulation proposed by Schneider [22], as expressed by Eq. (14) and plotted in Fig. 1a for different values of temperature:

$$\sigma(T) = \frac{3\varepsilon_c f_c^T}{\varepsilon_{c1}^T\left[2 + \left(\frac{\varepsilon_\sigma}{\varepsilon_{c1}^T}\right)^3\right]} \quad (14)$$

being f_c^T and $\varepsilon_{c1}{}^T$ the cylindrical compressive strength and the strain at the peak stress at temperature T, respectively.

The strain at the peak stress can be expressed by means of the expression suggested by Franssen [23], as reported in Eq. (15) and plotted in Fig. 1b:

$$\varepsilon_{c1}^T = 2.5\cdot10^{-3} + 4.1\cdot10^{-6}(T - 20) + 5.5\cdot10^{-9}(T - 20)^2 \le 10\cdot10^{-3} \quad (15)$$

In EC2's model, although the strain $\varepsilon_{\sigma,tr,cr}$ lumps together all strain components except for the free thermal strain, it is once again expressed by means of Eq. (14), but much larger values of the strain at the peak stress $\varepsilon_{c1}{}^T$ are adopted with respect to those suggested by Franssen [23]. In this way, all the load-induced components of strain are implicitly taken into account by increasing concrete deformability.

The descending branch in EC2's model can be expressed by either a linear or a non-linear curve (this latter being implemented in the present study) from the compressive strength f_c^T to zero when the ultimate strain $\varepsilon_{cu}{}^T$ is attained (Fig. 2).

In Fig. 1b the comparison among the values of $\varepsilon_{c1}{}^T$ provided by EC2 and by Eq. (15) [23], and the peak values of the load-induced strain $\varepsilon_{\sigma,tr,cr,peak}$ evaluated according to the three explicit models is presented. It is worth observing that up to 500 °C, the peak strains $\varepsilon_{\sigma,tr,cr,peak}$ evaluated according to Models 1 and 2 are close to each other and higher than both the peak strains $\varepsilon_{c1}{}^T$ (EC2, Model 4) and $\varepsilon_{\sigma,tr,cr,peak}$ of Model 3: the deformability of Models 1 and 2 in the ascending branch is larger than that of Models 3 and 4.

In Fig. 1c the initial tangent stiffness of the stress – load-induced strain relation, $\sigma(\varepsilon_{\sigma,tr,cr,})$, according to the different models is shown, while in Fig. 1d the same values are normalised with respect to the tangent stiffness of Model 4. It is clear that up to 600 °C Model 4 exhibits the largest stiffness, while Models 1 and 2 are very close and characterized by the largest deformability. For higher values of temperature, the situation strongly changes, even though stiffness becomes quite negligible (less than 5% of the value at room temperature). As for the values of f_c^T and $\varepsilon_{cu}{}^T$, reference can be made to the provisions of EC2 [9]. In Fig. 2a–f, the stress – load-induced strain diagrams obtained via the four models

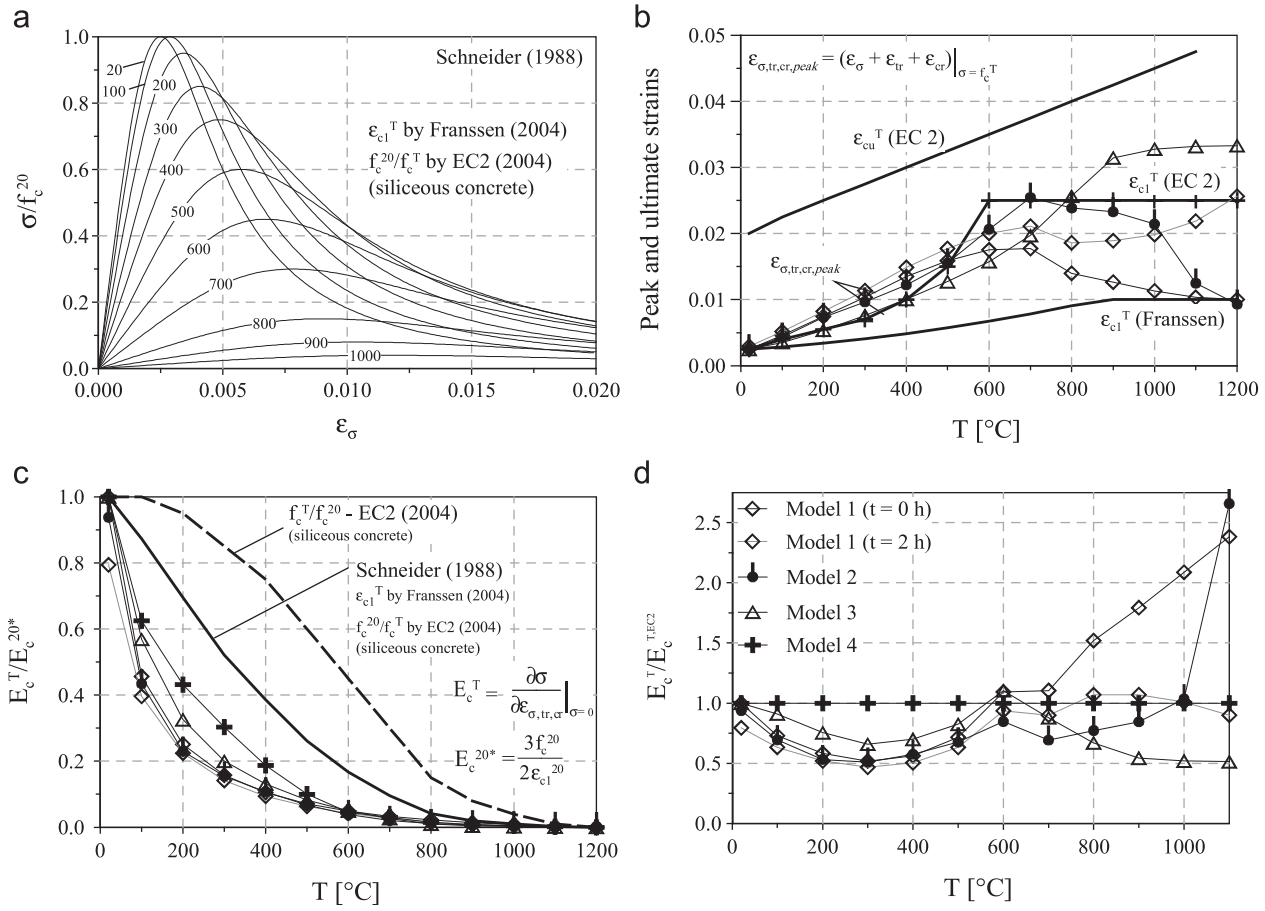

Fig. 1. (a) Stress – instantaneous load-induced strain curve by Schneider [22], Eq. (14); (b) peak strain ε_{cl}^T, peak load-induced strain $\varepsilon_{\sigma,tr,cr}$ according to the three explicit models, and ultimate strain ε_{cu}^T; (c) initial tangent stiffness of the stress-load induced strain curves; and (d) initial tangent stiffness according to the three explicit models, normalised with respect to the stiffness according to [9]. (For the legend see inset in (d)).

for different temperatures are shown, together with the instantaneous stress–strain law by Schneider [22].

3. Steel behaviour at high temperature

The total strain in heat-exposed steel consists of three components: (a) *thermal strain*, (b) *instantaneous stress-related strain* and (c) *creep strain*. In the following, the instantaneous stress-related strain and the thermal strain were evaluated according to EC2.

Experimental results reported in the literature show the occurrence of creep phenomena [21,24], which become significant only for very high temperature and loads applied for long periods. Hence, this contribution is generally neglected [12], also because it is partially taken into account (implicitly) in the constitutive law given by EC2.

4. Finite element analysis

In order to investigate the structural implications of the four presented concrete models on the response of rather simple heat-exposed R/C members, such as beams and columns, a FE code for the thermo-mechanical analysis of beam elements has been developed by using a FORTRAN solver, together with the pre- and post-processor GID.

Generally speaking, the problem of heat-exposed R/C members involves a hygro-thermo-mechanical problem, in which the three layouts are strongly related. In the last years, as a matter of fact, a few authors have developed numerical analyses regarding all the aforementioned aspects [2,20,25], leading to complex mathematical models capable of capturing: (a) the pore pressure field due to mass transport and water vaporisation; (b) the thermal field considering the heat transferred by the fluids in relative motion with respect to the solid skeleton; and (c) the development of stresses induced by restrained thermal dilation and external loads.

These analyses proved to be effective in predicting the experimental behaviour and in getting a deeper insight into the different physical phenomena, but are rather time-consuming and, therefore, not very appealing from the structural point of view. Hence, in the present study, another approach has been pursued. As in the case of previous works by other authors [4,13,14], the basic assumption that thermal behaviour influences mechanical behaviour – but not vice versa – is retained. Moreover, since the spalling phenomenon is not considered (also in view of the experimental results considered in the following), the hygral layout is completely disregarded. As a consequence, the implemented thermo-mechanical analysis is sequentially-coupled, and the solution of the problem can be subdivided into two parts [4,13,14]: thermal and mechanical analyses.

4.1. Thermal analysis

In the thermal analysis, the effect of heat on the cross section is applied via convection and radiation, while conduction is considered inside the cross section. The three phenomena are governed by Newton's, Stefan–Boltzmann's and Fourier's laws, respectively.

The temperature is assumed to be uniform along the length of the member as in [4,13,14]; hence, the thermal problem is reduced to a 2D problem.

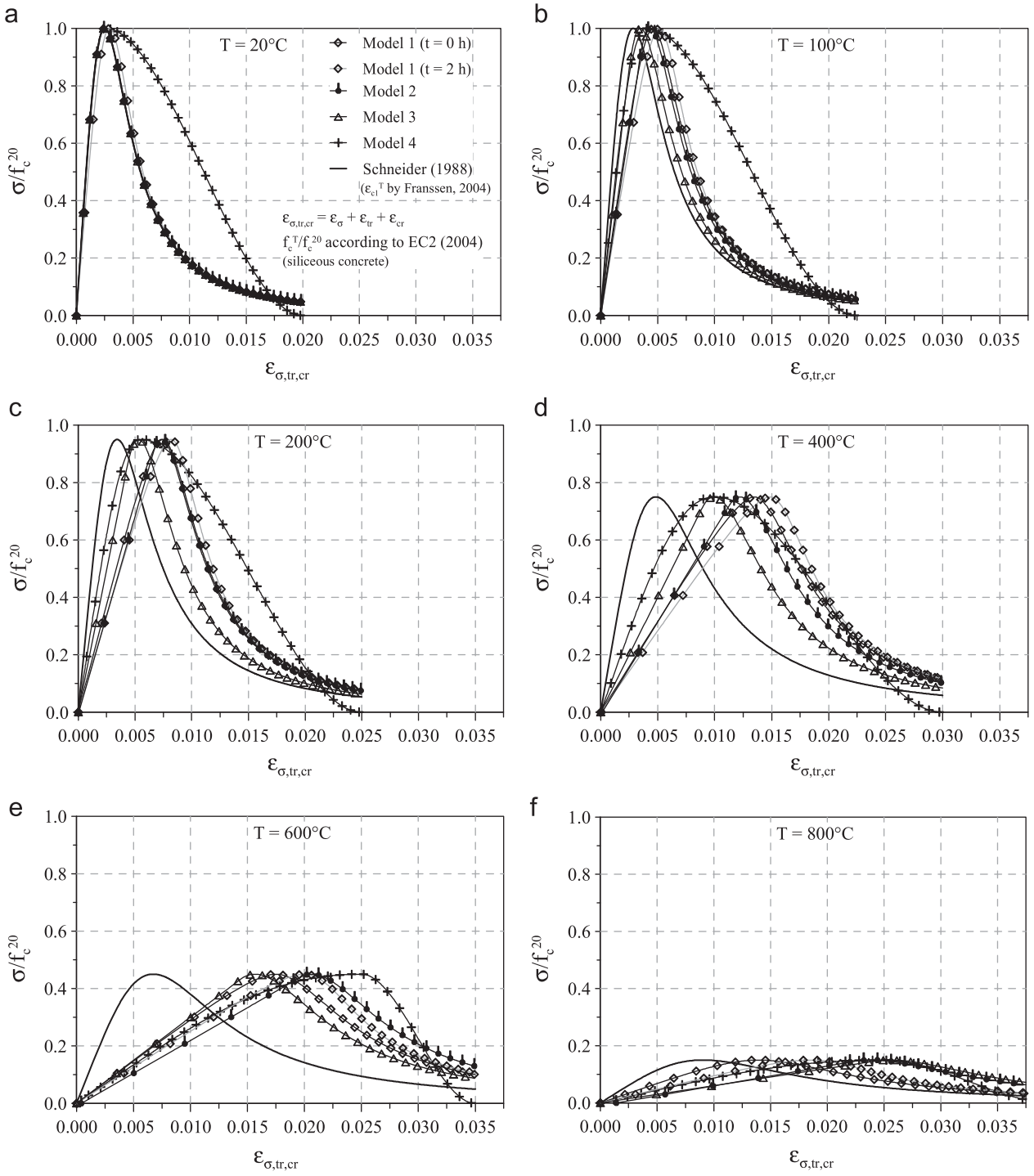

Fig. 2. Stress – load-induced strain relation, $\sigma(\varepsilon_{\sigma,tr,cr})$, for concrete in compression according to the four models together with Schneider's basic law at different temperatures T. For the legend see the inset in (a).

In the present study, triangular elements with three nodes (hence, with linear shape functions) have been used. The Gauss quadrature was implemented by using three integration points in the 2D domain and two points for each side of the triangle in the 1D contour-domain. The non-heated boundaries are considered adiabatic: this is a conventional choice that proved to be conservative [26], because it leads to higher temperatures inside the section core.

The backward Euler method was used for the integration in the time domain, as in [2,25]. Being concrete thermal properties functions of temperature, the problem is non-linear, and its solution is found by iteration. Within this procedure, convergence was evaluated by checking the maximum error among all nodal temperatures of the mesh.

As regards the variation of concrete thermal properties with temperature, the formulations proposed by EC2 have been used. As it is usually done in R/C members, the thermal analysis was performed neglecting the presence of the steel bars [13,14].

To validate the developed code in performing thermal analysis, a square concrete section (30×30 cm^2), heated on four sides according to the ISO 834 Standard Fire has been numerically modelled, and the results have been compared with the temperature

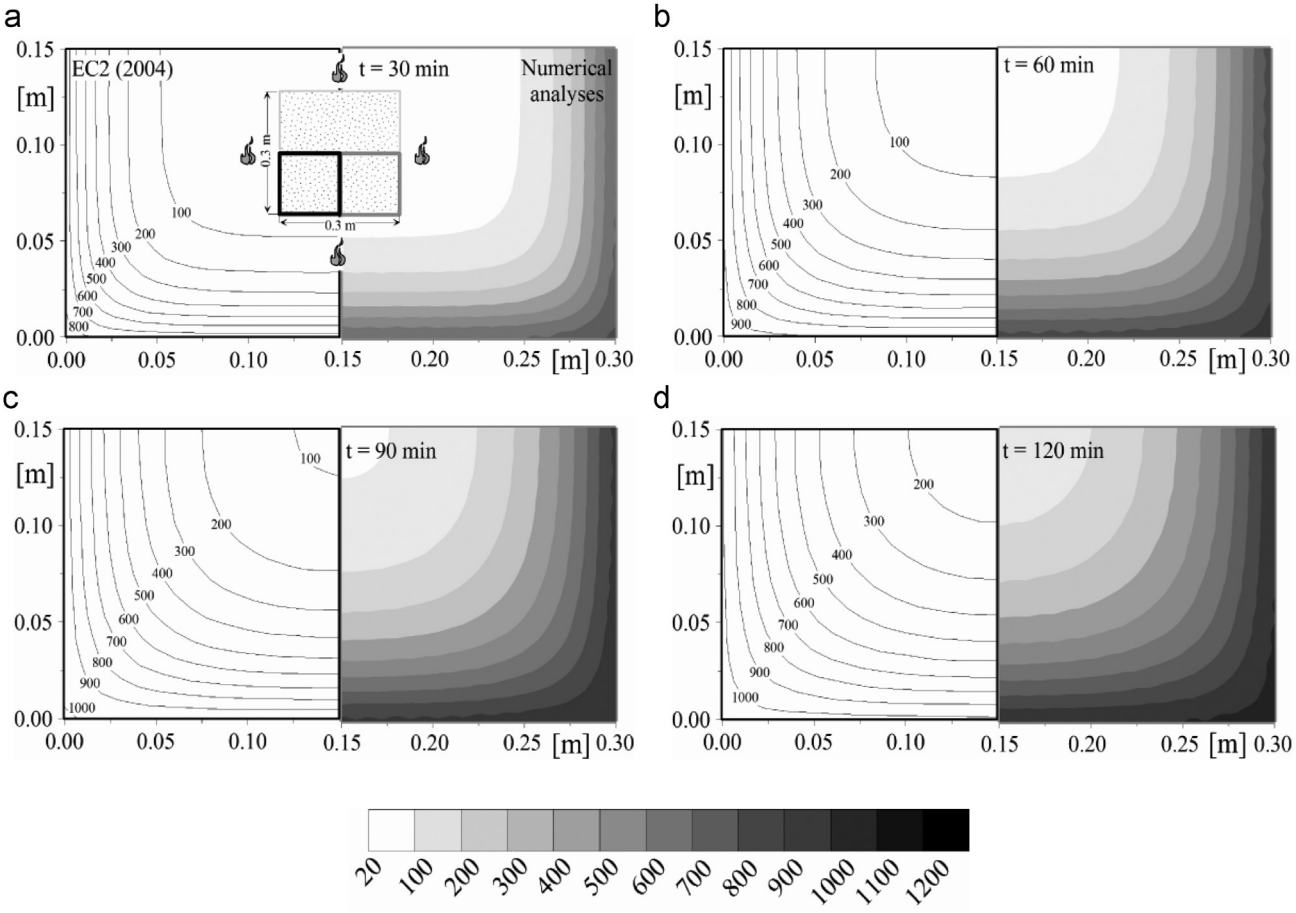

Fig. 3. Square column (30×30 cm^2) heated on 4 sides: comparison between the thermal fields evaluated numerically (right) and given by EC2 [9] (left), at different fire durations: 30 (a), 60 (b), 90 (c) and 120 min (d).

profiles given in Annex A of EC2, as shown in Fig. 3. The role of the moisture is taken into account in the simplified way suggested by EC2, through the introduction of a peak in the specific heat between 100 and 200 °C. The comparisons shown in Fig. 3 indicate that the temperature profiles evaluated by means of the developed code are in very good agreement with those provided by EC2, thus confirming the validity of the code implemented for the purpose of the analyses presented in the following.

4.2. Mechanical analysis

Once the thermal analysis has been carried out, and the temperature is known at any given point of the cross section and for any given fire duration, the mechanical analysis is performed. The traditional assumptions concerning slender Euler–Bernoulli beam elements are mantained as in [14,27], namely: (a) plane sections remain plane, and (b) negligible shear deformation of the sections. In all cases, perfect steel-to-concrete bond is assumed, and the contribution of concrete in tension is neglected.

The deformed shape of the beam elements is a function of the 6 nodal degrees of freedom (two translations, and one rotation per node for plane beam elements) via the usual linear and cubic shape functions for the axial and flexural behaviours, respectively.

The stiffness matrix and the vector of the equivalent nodal forces are worked out by means of the traditional beam FE theory for linear elastic problems, taking into account the role played by the coupling between axial force N and bending moment M that typically occurs in the case of non-linear constitutive laws [27].

Once the stiffness matrix and the vector of equivalent nodal forces are assembled, the equilibrium of the structure can be imposed by the well known system of equations reported in Eq. (16):

$$\left(\underline{\underline{K}}_E - \underline{\underline{K}}_G\right)\underline{q} = \underline{F}_{im} + \underline{F} \rightarrow \underline{\underline{K}}\underline{q} = \underline{f} \tag{16}$$

where $\underline{\underline{K}}_E$ is the structural stiffness matrix, $\underline{\underline{K}}_G$ is the geometric matrix ([4,27], taking into account second-order effects because of the coupling between axial loads and flexural deformations/displacements), $\underline{q}$ is the vector containing the nodal translations and rotations, $\underline{F}_{im}$ is the vector of the nodal forces equivalent to the restrained thermal strains, $\underline{F}$ is the vector of the external nodal forces. Clearly, the collapse of a structural element is determined when static equilibrium is no longer possible, namely when the global stiffness matrix $\underline{\underline{K}}$ becomes singular for the first time (*global failure*).

The elastic modulus E is defined as secant modulus, that is the ratio between the applied stress σ and the total load-induced strain $\varepsilon_{\sigma,tr,cr}$. Obviously, E is a function of both temperature and stress, making the structural problem non-linear; hence, the solution requires an iterative process. The convergence has been evaluated by checking, at each step i of the analysis, the difference between the external and the internal forces, $\underline{f}$ and $\underline{\underline{K}}\,\underline{q}$, respectively. As regards the convergence of the non-linear problem, the use of the secant elastic modulus guarantees a higher stability with respect to an approach based on the tangent elastic modulus, which is, on the contrary, faster.

The integration along the beam axis was performed by Gauss quadrature with three points, while the integration on the section was performed with three Gauss points per triangular element (the same mesh of the thermal analysis was used).

For the numerical analyses, a generic structural member is subdivided into different longitudinal segments (at least six beam elements).

5. General considerations on the structural behaviour of R/C columns

To draw some general considerations on the different models presented in the previous sections, and to assess the reliability of 1D numerical analyses in understanding the thermal and mechanical response of R/C members, some real columns tested in the framework of different experimental campaigns on full-scale specimens are simulated; the results of the numerical simulations are, then, compared with the test results. Note that (a) all the tests considered in the following were carried out under a monotonic fire scenario (ISO 834, ASTM E-119 or similar) with no cooling phase, and (b) failure was considered to be attained whenever the testing machine was no longer able to maintain the load applied on the specimen. Therefore, all the considerations that will be drawn are relevant for problems where collapse is likely to occur during the heating phase. Besides, three of the four models that will be used for simulating concrete behaviour are intended for the heating phase only, with no clear indication on concrete behaviour upon cooling. It is worth noting that the columns examined in the following subsections did not exhibit significant spalling during the heating phase: therefore, no section reductions were taken into account in the thermo-mechanical analyses.

5.1. Concentric load

The first set of experimental data consists of three R/C columns made of siliceous concrete, with square/rectangular section, tested by Lie and Irwin [28]. In Fig. 4 the cross section and the position of the reinforcing bars as well as the reference points for the temperature measurements are shown for each column.

Columns 1 and 2 were heated along four sides following the ASTM E-119 temperature-time curve, while Column 3 was subjected to ASTM E-119 for about 30 min, and then to a temperature-time law approximated by equation $T = 14.88t + 831.8$, with T in °C and t in hours (see Fig. 5a). The columns were clamped at the two ends, with a concentric load applied before the fire and maintained constant throughout the test. The data of the different tests are summarised in Table 1.

In Fig. 5c and e, the temperature measured experimentally and evaluated numerically at the reference points for the two types of cross section (Columns 1, 2 and Column 3) are shown as a function of the fire duration: the agreement between numerical analyses and experimental results is in all cases rather good, especially beyond 200 °C. Note that the experimental temperature-time plots in Fig. 5c were obtained by averaging the temperatures at different points of the section of Columns 1 and 2 (that are nominally identical as for geometry and boundary conditions) along the height of the columns.

In Fig. 5b, d and f, the evolution of the elongation is reported for the three columns, according to both the experimental measurements (grey line) and the numerical simulations (black line). Both first-order (black dashed lines) and second-order (black continuous lines) calculations were performed. For these three examples, moreover, a structural analysis disregarding transient and creep strains has been performed, by using Schneider's basic law. This last model is indicated in the figures as "No LITS" and allows to highlight the role played by transient and creep strains.

Looking at the plots representing the axial elongation, it is worth noting that the general trend obtained assuming the different models is the same. The differences among the models are minimal in the ascending branch, where the deformations are controlled by the thermal dilation, while they become sizable after the peak, where the effect of loading and reduced axial stiffness prevails. Rather good agreement is obtained both in terms of displacements as well as with regards to the time to failure, as also shown in Table 2. The lines representing the experimental data, in fact, lie inside or very close to the region bounded by the numerical results obtained with the four considered models (grey shaded areas in Fig. 5b, d and f).

Nonetheless, the differences among the models in the time to failure are much less sizable than the differences in terms of displacements. Eventually, Fig. 5 shows that the introduction of second-order effects via the geometric stiffness matrix $\underline{\underline{K}}_G$ brings in an important reduction of the failure time, in spite of the clamped ends and the limited height (3.8 m). Comparing the four models, it is plain to see that the stiffer the model, the lower the decrease of time to failure caused by second-order effects. Notably, since the axial load is concentric and the columns are heated on four sides, there are no lateral deflections prior to collapse; therefore, the ultimate situation is attained as a pure bifurcation-type buckling instability, that is triggered by the singularity of the stiffness matrix. Obviously, this situation is an idealised representation of what happens in reality, where (a) the temperature inside a furnace and the temperature profiles inside the section are surely not perfectly symmetric; and (b) accidental, though small, eccentricities of the axial loads are always present.

5.2. Eccentric load

A series of full-scale tests on heated R/C columns, made of siliceous concrete, subjected to both concentric and eccentric loads were carried out at the Technical University of Braunschweig [29]. Three full-scale tests involving columns heated according to the ISO 834 Standard Fire and axially loaded with different values of

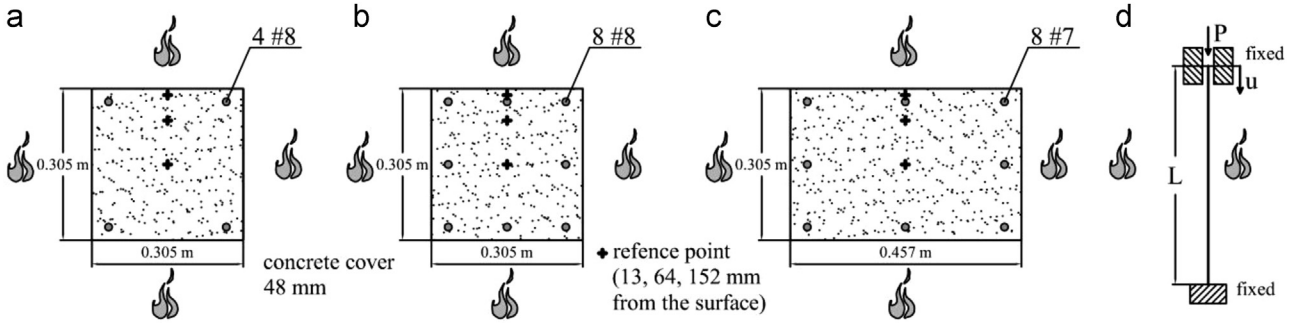

Fig. 4. Cross section, arrangement of the bars and location of the reference points for the measurement of temperature – (a) Column 1, (b) Column 2, (c) Column 3; (d) boundary conditions; Lie and Irwin [28].

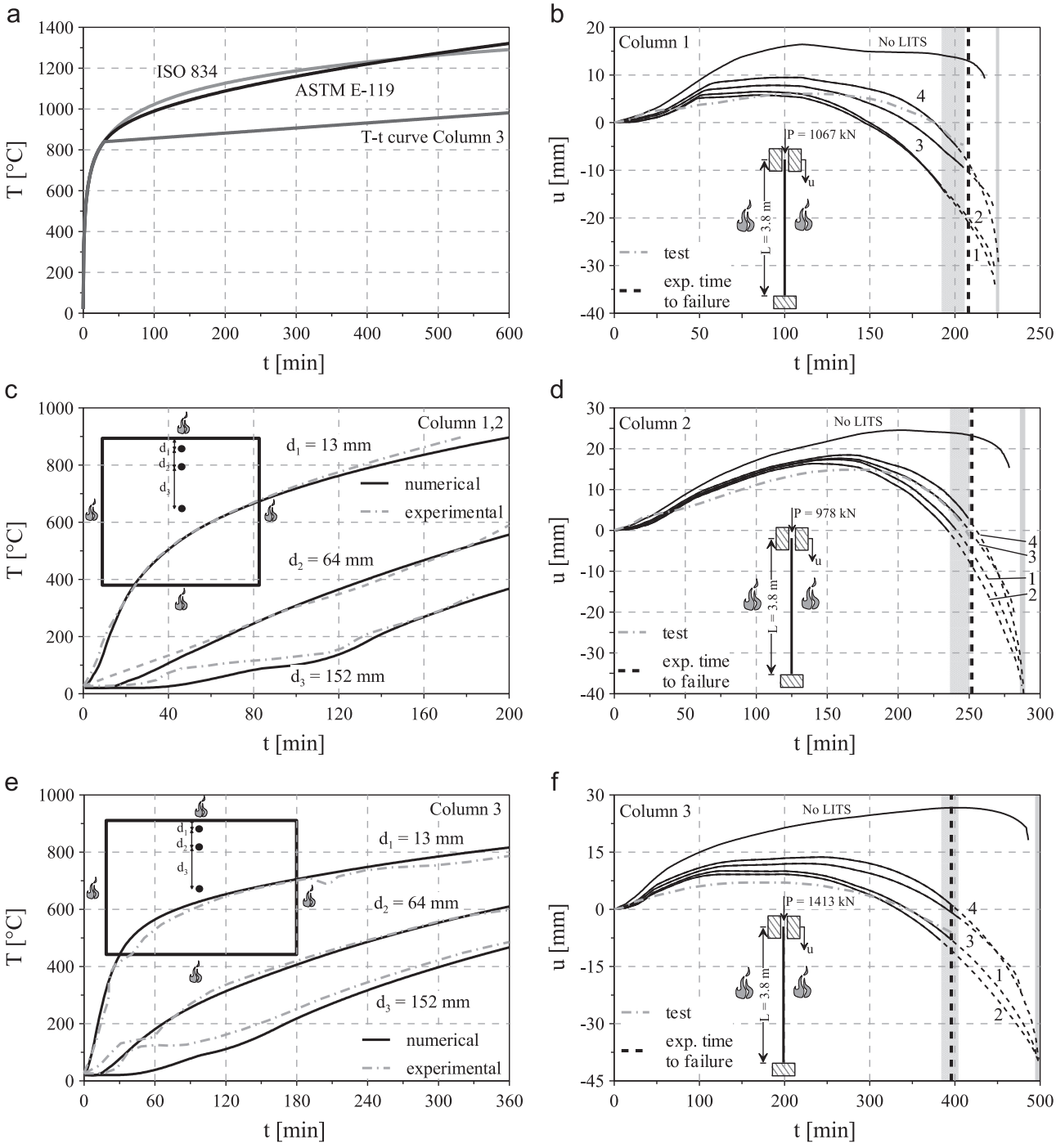

Fig. 5. Typical temperature-time curves (a), plots of the temperature development as a function of time in three reference points – (c) Column 1,2, (e) Column 3 – and of the axial elongation during heating – (b) Column 1, (d) Column 2, (f) Column 3 – according to the four models.

Table 1
Geometrical and mechanical parameters of the columns tested by Lie and Irwin [28].

Column	Dimensions (mm × mm)	L (m)	f_y (MPa)	f_c (MPa)	Load (kN)	e (mm)	Failure (min)
1	305 × 305	3.8	444	36.1	1067	0	208
2	305 × 305	3.8	444	42.6	978	0	252
3	305 × 457	3.8	414	42.5	1413	0	396

Table 2
Time to failure according to the experimental results [28] and to the four numerical models. t, t_{exp} = numerical, experimental time to failure.

	Column 1		Column 2		Column 3	
	t (min)	t/t_{exp}	t (min)	t/t_{exp}	t (min)	t/t_{exp}
Model 1	195	0.94	240	0.95	395	1.00
Model 2	192	0.92	236	0.94	384	0.97
Model 3	205	0.99	245	0.97	405	1.02
Model 4	202	0.97	249	0.99	399	1.01
Experimental	208	–	252	–	396	–

Table 3
Geometry and mechanical properties of the columns tested by Hass [29].

Column	Dimensions (mm × mm)	L (m)	f_y (MPa)	f_c (MPa)	Load (kN)	e (mm)	Failure (min)
Hass 1	300 × 300	3.76	487	24.1	710	30	86
Hass 16	300 × 300	4.76	462	30.7	460	90	75
Hass 21	300 × 300	3.80	418	33.2	780	50	125

eccentricity were simulated numerically. The geometry and the mechanical properties are reported in Table 3, while the arrange-ment of the bars and the boundary restraints are shown in Fig. 6.

The results concerning the evolution of the first-order axial elongation at mid-height are shown in Fig. 7a, c and e (black dashed lines). As in the columns tested by Lie and Irwin, Models 1 and 2 lead to very similar results, and are characterized by the largest deformability, while Model 4 is characterized by the stiffest response. For each model, the introduction of second-order effects (black continuous lines) causes a very sizable decrease of the fire resistance. Also in this case, the differences among the four models are minimal, especially in the ascending branch. Moreover, both first-order and second-order calculations bring in time to failure values which are always comprised within rather narrow bands (grey shaded areas in Fig. 7).

Table 4 shows the comparison among the experimental time to failure (that is represented with vertical dashed lines in Fig. 7) and those evaluated numerically. Fig. 7b, d and f show the results concerning the same columns in terms of lateral deflection at mid-height. The considerations made with reference to the axial displacement are still valid. In this case, the failure becomes more evident, with the typical increase of the lateral displacement rate (*runaway failure*), particularly when second-order effects are taken into account. Contrary to the case of columns subjected to concentric loads, the lateral displacement is not zero, even for low values of fire duration.

The role played by second-order effects and decay of the bearing capacity is clearly shown in Fig. 8, separately for Models 1–4 in the case of the reference column “Hass 1”.

Fig. 8a and b show the acting bending moment and the bearing capacity in bending of the most stressed section as a function of the fire duration: in the first 20 min of heating, the acting bending moment, including second-order effects, is rather constant (=23.4–25.9 kNm), showing that second-order effects are limited; beyond 30 min, the bending moment reaches a value close to 28 kNm for all the Models, while, at failure, it ranges from 92 (Model 3) to 104 kNm (Model 1).

Therefore, at impending collapse, the moment is up to 4.5 times the initial value. On the other hand, the sectional bearing capacity, for the imposed axial load of 710 kN, ranges initially between 162 (Model 1, 2, 3) and 164 kNm (Model 4) and becomes equal to the external moment at the time to failure (decrease of 36–43%).

Fig. 8a and b clearly show that: (a) the decay of the sectional bearing capacity and the increase of the acting bending moment due to second-order effects both play an important role (probably the latter more than the former) in triggering the collapse; (b) the resistant moments evaluated according to the explicit models are very close to each other, while EC2's model leads to slightly larger values due to the more soft post-peak branch (see Fig. 2); (c) the differences in terms of time to failure among the four models are mostly related to the increase rate of second-order effects (hence, to the deformability) rather than to strength. Although Model 3 leads to the lowest value of resistant moment during heating, in fact, it leads to the highest fire resistance among the explicit models thanks to its larger stiffness.

Fig. 8a also shows that for the models characterized by the largest deformability (Models 1 and 2) the dramatic increase of acting bending moment begins for lower fire durations than for Model 4 (that is the stiffest): as a consequence, the structural behaviour seems to be controlled mainly by the ascending branch of the constitutive law.

An alternative representation of the role played by second-order effects and decay of the bearing capacity is given in Fig. 8c–f, where the *M–N* interaction envelopes and the points representing the external forces are plotted as a function of the fire duration for Models 1–4. Once more, it is confirmed that (a) the increase of the acting bending moment and the decrease of the bearing capacity in bending both play a significant role; (b) no sizable difference can be observed among the different models in terms of bearing capacity.

Finally, the curve representing the bending moment due to the applied loads intersects the resistant moment with an almost vertical tangent; this means that the time to failure is more sensitive to the correct evaluation of second-order effects (hence, to concrete deformability), rather than to refinements in the calculation of the resistant moment.

6. Comparisons between experimental and numerical results

So far, all the considerations were focused on the differences among the four constitutive models. It is now interesting to compare the overall ability of the models to correctly predict the time to failure measured during full-scale tests. To this end, the structural behaviour of 55 R/C columns tested in the laboratories of the Technical University of Braunschweig (39 tests) [29] and of the University of Ghent (16 tests) [30] was simulated numerically, and the time to failure was calculated according to the four models taking into account second-order effects. Significant spalling occurred only in four cases (among the columns tested at the University of Ghent): those columns were not considered in the simulations.

The numerical results were obtained on the basis of the nominal values of the mechanical properties, as declared by the

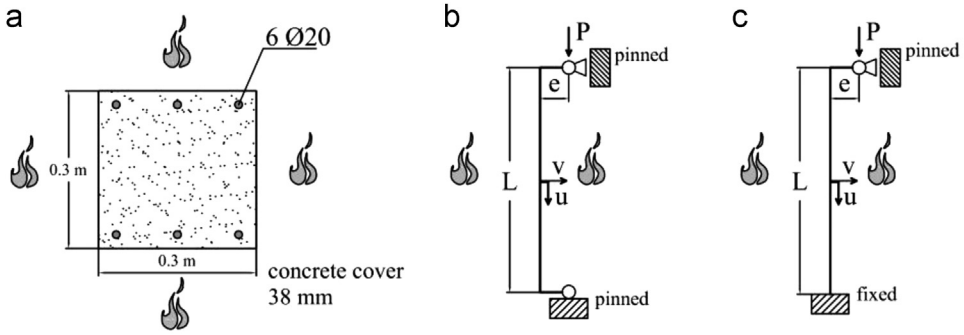

Fig. 6. Cross section and rebars layout of the three columns (a); boundary restraints of columns “Hass 1” and “Hass 16” (b), and of column “Hass 21” (c); Hass [29].

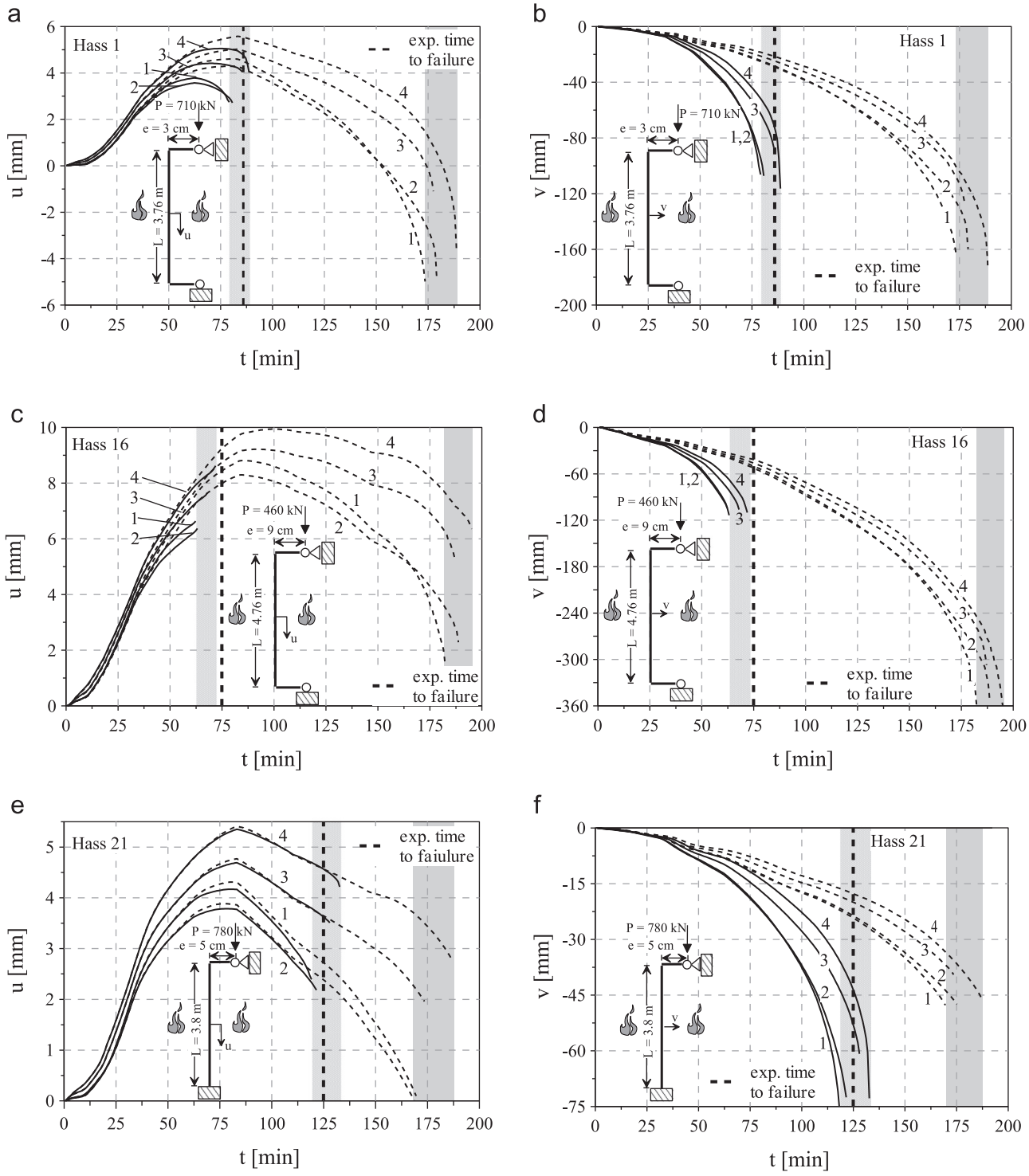

Fig. 7. Plots of the axial deformation – (a) Hass 1, (c) Hass 16, (e) Hass 21– and of the lateral deflection – (b) Hass 1, (d) Hass 16, (f) Hass 21 – as a function of time, evaluated numerically according to the four models.

Table 4
Time to failure according to the experimental results [29] and to the four numerical models. t, t_{exp} = numerical, experimental time to failure.

	Hass 1		Hass 16		Hass 21	
	t (min)	t/t_{exp}	t (min)	t/t_{exp}	t (min)	t/t_{exp}
Model 1	79	0.92	63	0.84	119	0.95
Model 2	81	0.94	64	0.85	122	0.98
Model 3	86	1.00	68	0.91	128	1.02
Model 4	89	1.03	73	0.97	133	1.06
Experimental	86	–	75	–	125	–

authors of the tests. Where no clear indications were provided, reference was made either to the reference values of Models 1, 2 and 3, or to the provisions of EC2 for Model 4.

The results are presented through the ratio between the calculated time to failure (t_{model}) and the time to failure measured in the tests (t_{test}). The values of the ratio t_{model}/t_{test} were calculated separately for each of the four models, and four statistical distributions were obtained (Fig. 9; range 0–2). Clearly, the results characterized by $t_{model}/t_{test} \leq 1$ are on the safe side.

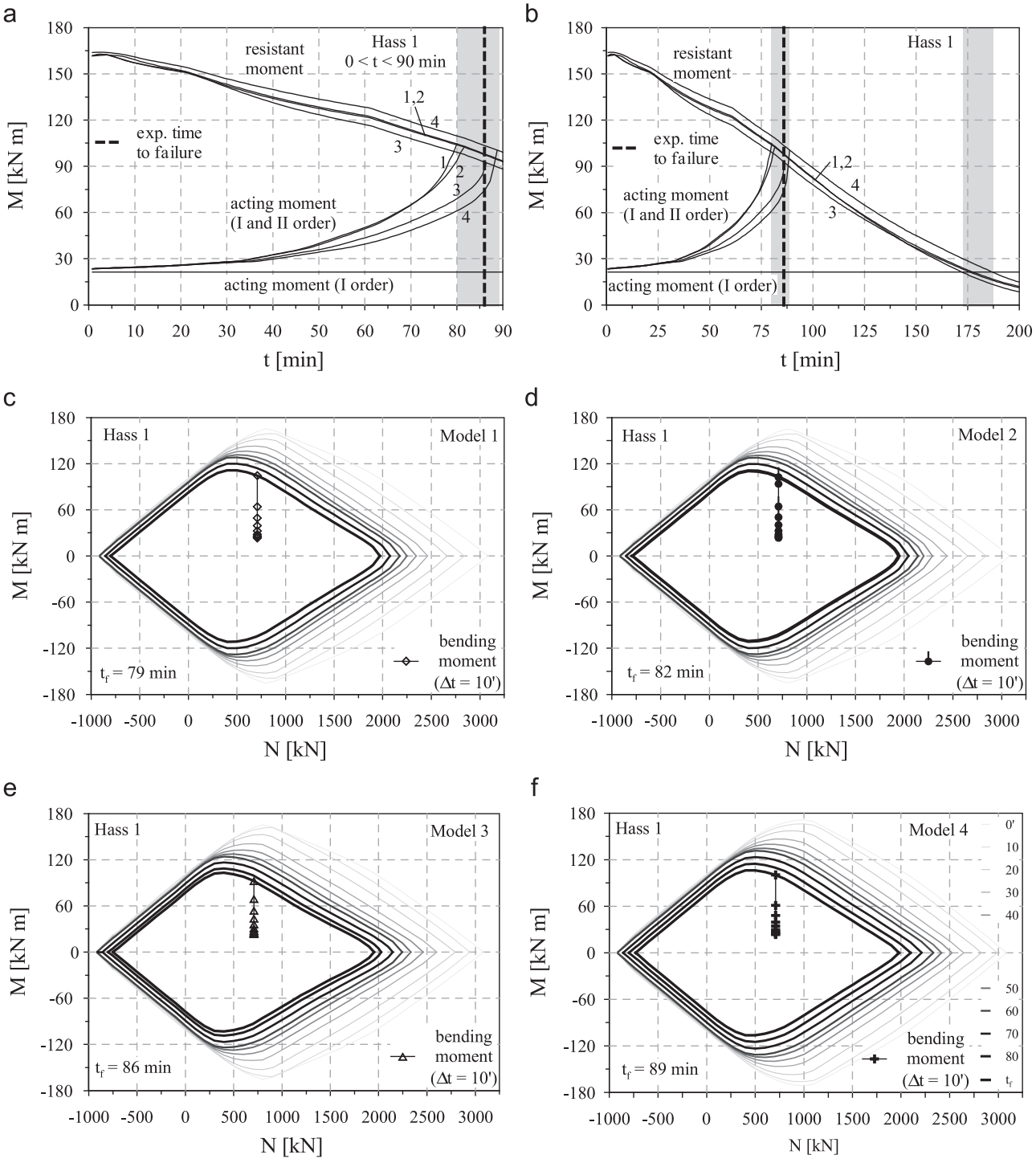

Fig. 8. Column Hass 1: plots of the resistant and of the acting moments as functions of time – (a) $t < 90$ min and (b) full plot; (c–f) plots of the M–N interaction envelope during heating, according to the four models.

The numerical simulations taking into account creep and transient strains tend to give smaller values of fire resistance than those measured experimentally; in any case, the overall agreement between the numerical analyses and the experimental results is satisfactory. Among the four models, Models 1 and 2 are the most conservative, with a mean value of t_{model}/t_{test} equal to 0.83; Model 4 brings in the best agreement (mean value of 0.96), while Model 3 is in an intermediate position (mean value of 0.91).

The standard deviations range from 0.25 to 0.27 and are similar to those commonly found in the literature. Clearly, better results could be obtained if the temperature-dependant mechanical properties of concrete used in the simulations were calibrated on suitable experimental data; herein, reference was made in all cases to the standard decay curves provided in EC2.

Fig. 10a and b show the ratio between the values of time to failure evaluated according to the explicit models (Models 1, 2 and 3) and those by EC2 (Model 4). These populations of data ($t_{Model1,2,3}/t_{Model4}$) have very low standard deviations (from 0.03 to

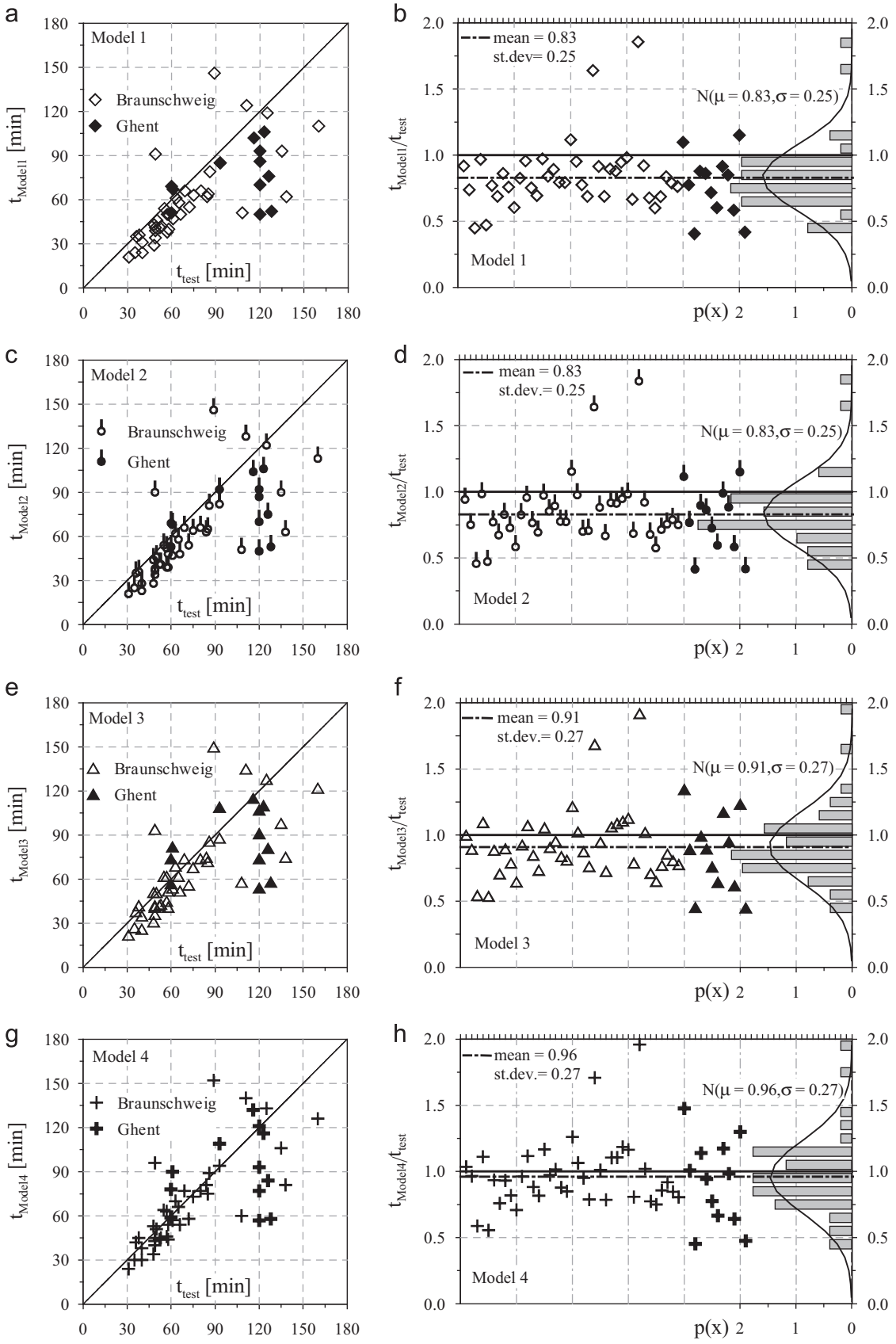

Fig. 9. Numerical simulations of the columns tested at Braunschweig [29] and at Ghent [30]: (a, c, e, g) values of the time to failure according to the four models as functions of the experimental ones; (b, d, f, h) values of the time to failure according to the four models normalised with respect to the experimental ones and statistical distribution of the populations of data.

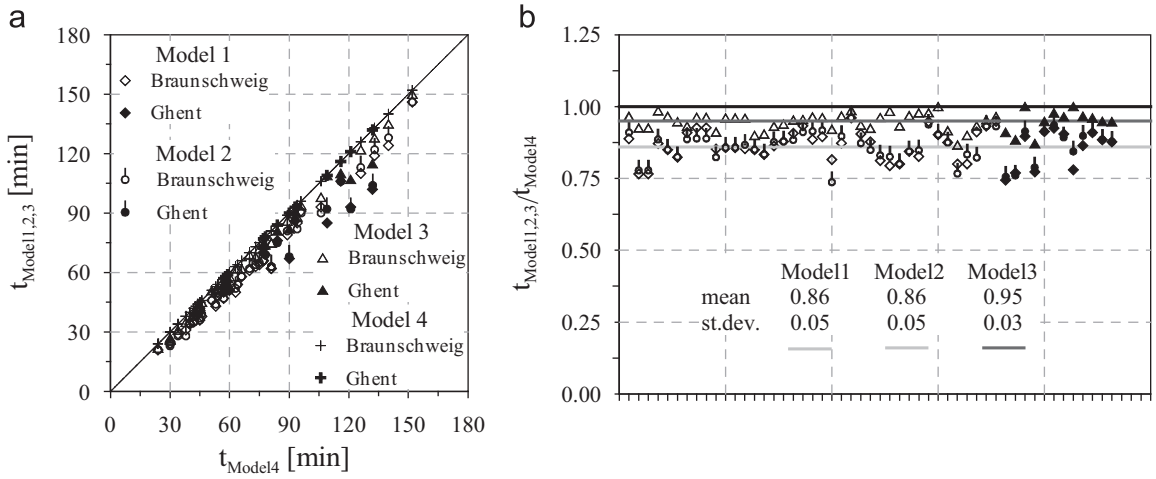

Fig. 10. Numerical simulations of the columns tested at Braunschweig [29] and at Ghent [30]: (a) values of the time to failure according to the explicit models as functions of those evaluated according to EC2 model; and (b) values of the time to failure according to the explicit models normalised with respect to the EC2 ones.

0.05) and mean values of 0.86 (Models 1 and 2) and 0.95 (Model 3). Hence, Anderberg and Thelandersson's and Khoury and Terro's models give values of time to failure 14% smaller than EC2 (on the average), while Schneider et al.'s model only 5% smaller, being these trends characterized by great repeatability.

It is worth noting that the differences between the numerical predictions and the test results (represented by standard deviations in excess of 0.20) are surely partly due to the scattering of the test results alone; as a matter of fact, there are several cases where nominally-identical test specimens give different results.

7. Conclusions

In the present paper, the results obtained via a Beam Finite Element code aimed at the thermo-mechanical analysis of reinforced concrete members in fire are presented. Four different constitutive models for concrete compressive behaviour in hot conditions were considered, in order to highlight the differences between explicit and implicit formulations of the stress–strain relationship.

On the basis of the numerical modelling of a significant number of real-scale tests on R/C columns subjected to Standard Fire, some general conclusions can be drawn:

- A Beam Finite Element approach, which considers both transient and creep deformations, and second-order effects allows to perform numerical analyses consistent with the experimental behaviour of concrete in hot conditions, for both explicit and implicit constitutive models;
- Second-order effects sizably affect the time to failure of R/C members subjected to axial load (with or without eccentricity), even in relatively short columns (3–6 m), this being the reason why concrete stiffness is a key parameter;
- The time to failure (thus, the fire resistance) increases with concrete stiffness, because the decrease of the resistant moment is more than offset by the reduction of second-order effects;
- The explicit models by Anderberg and Thelandersson, and by Khoury and Terro lead to very similar results and are characterized by a larger deformability and by smaller values in terms of fire resistance (expressed in terms of time to failure) with respect to the other models;
- The model proposed by EC2 – Fire Design is the stiffest and leads to the highest values of time to failure;
- In terms of agreement between numerical and experimental results, the model proposed in EC2 – Fire Design, that is the most appealing from the designer's point of view because of its simplicity in implementation, appears to be the best; it is worth noting, however, that the EC2 provisions could have been calibrated on the same database that was used in the present paper.

Generally speaking, a Beam Finite Element model proved to be reliable for all the four constitutive models, leading to a rather good agreement with the experimental results. It is reasonable to assume that even better results could be obtained, if the implemented constitutive law for concrete was calibrated on the basis of experimental investigation.

Acknowledgements

Prof. Luigi Cedolin is thanked for the fruitful discussions on the basic aspects of structural stability. The authors are also grateful to Prof. Pietro G. Gambarova for the valuable suggestions in the interpretation of the results, and for helping in improving the manuscript.

References

[1] G.A. Khoury, Effect of Fire on Concrete and Concrete Structures, Prog. Struct. Eng. Mater. 2 (2000) 429–447.
[2] G.A. Khoury, C.E. Majorana, F. Pesavento, B.A. Schrefler, Modelling of heated concrete, Mag. Concr. Res. 54 (2) (2002) 77–101.
[3] D. Gawin, P. Pesavento, B.A. Schrefler, What physical phenomena can be neglected when modelling concrete at high temperature? A comparative study. Part 2: Comparison between models, Int. J. Solids Struct. 48 (2011) 1945–1961.
[4] V. Kodur, M. Dwaikat, N. Raut, Macrospopic FE model for tracing the fire response of reinforced concrete structures, Eng. Struct. 31 (2009) 2368–2379.
[5] S.S. Huang, I. Burgess, Z.H. Huang and P. Plank, Effect of transient thermal strain on the buckling of slender concrete and concrete-filled columns in fire, in: Proceedings of the Fifth International Conference on Structures in Fire –SiF'08, Singapore, May 28–30, 2008, pp. 594–605.
[6] Y. Anderberg, S. Thelandersson, Stress and Deformation Characteristics of Concrete at High Temperatures-2. Experimental Investigation and Material Behaviour Model, Lund Institute of Technology, Lund (Sweden), 1976, Report No. 34, Division of Structural Mechanics and Concrete Construction.

[7] M.J. Terro, Numerical modelling of the behaviour of concrete structures in fir, ACI Struct. J. 95 (2) (1998) 183–193.
[8] U. Schneider, M. Schneider, J.M. Franssen, Consideration of nonlinear creep strain of siliceous concrete on calculation of mechanical strain under transient temperatures as a function of load history, in: Proceedings of the Fifth International Conference on Structures in Fire – SiF'08, Singapore, May 28–30, 2008, pp. 463–476.
[9] EN 1992-1-2:2004, Eurocode 2-Design of concrete structures-Part 1–2: General rules-Structural fire design, European Committee for Standardization (CEN), Brussels, 2004.
[10] P. Bamonte, F. Lo Monte, Modeling R/C columns in fire according to different constitutive models for heated concrete, in: Proceedings of the Sixth International Conference Structures in Fire, SiF'10, East Lansing Michigan, USA, June 2–4, 2010, 320–327.
[11] Z. Huang, A. Platten, Nonlinear finite element analysis of planar reinforced concrete members subjected to fire, ACI Struct. J. 94 (3) (1997) 272–282.
[12] F. Biondini, A. Nero, Cellular finite beam element for nonlinear analysis of concrete structures under fire, J. Struct. Eng. ASCE 137 (5) (2011) 543–558.
[13] S. Bratina, B. Cas, M. Saje, I. Planinc, Numerical modeling of behavior of reinforced concrete columns in fire and comparison with Eurocode 2, Int. J. Solids Struct. 42 (2005) 5715–5733.
[14] M. Dwaikat, V. Kodur, A numerical approach for modeling the fire induced restraint effect in reinforced concrete beams, Fire Saf. J. 43 (2008) 291–307.
[15] K. Sidibé, F. Duprat, M. Pinglot, B. Bourret, Fire safety of reinforced concrete columns, ACI Struct. J. 97 (4) (2000) 642–647.
[16] K.H. Tan, C.Y. Tang, Interaction formula for reinforced concrete columns in fire condition, ACI Struct. J. 101 (1) (2004) 19–28.
[17] L.H. Han, Y.Q. Zheng, J.G. Teng, Fire resistance of RC and FRP-confined RC columns, Mag. Concr. Res. 58 (8) (2006) 533–546.
[18] A. Law, M. Gillie, Load induced thermal strain: implications for structural behaviour, in: Proceedings of the Fifth International Conference on Structures in Fire – SiF'08, Singapore, May 28–30, 2008, pp. 488–498.
[19] G.A. Khoury, Strain of heated concrete during two thermal cycles – Part 1, 2 and 3, Mag. Concr. Res. 58 (2006) 367–385 58, pp. 387 400, 58, pp. 421-435.
[20] Z.O. Bazant, M.F. Kaplan, Concrete at High Temperatures: Material Properties and Mathematical Models, Longman, Harlow, Essex, England, 1996.
[21] Y. Anderberg, The impact of various material models on structural fire behaviour prediction, in: Proceedings of the Fifth International Conference on Structures in Fire – SiF'08, Singapore, May 28–30, 2008, pp. 253–265.
[22] U. Schneider, Concrete at high temperatures–a general review, Fire Saf. J. 13 (1) (1988) 55–68.
[23] J.M. Franssen, Plastic analysis of concrete structures subjected to fire, in: Proceedings of the Workshop "Fire design of concrete structures: What now? What next?", Milan Italy, December 2–3, 2004, pp. 133–146.
[24] J. Rigberth, Simplified Design of Fire Exposed Concrete Beams and Columns, 2000, Report 5063, Department of Fire Safety Engineering, Lund University, Lund, Sweden, 88 pp.
[25] D. Gawin, P. Pesavento, B.A. Schrefler, What physical phenomena can be neglected when modelling concrete at high temperature? A comparative study. Part 1: hysical phenomena and mathematical model, Int. J. Solids Struct. 48 (2011) 1927–1944.
[26] K.H. Tan, Y. Yao, Fire resistance of four-face heated reinforced concrete columns, J. Struct. Eng. ASCE 129 (9) (2003) 1220–1229.
[27] P. Malerba, Analisi limite e non lineare di strutture in calcestruzzo armato: tecniche di calcolo manuale ed automatico, International Centre for Mechanical Sciences.(CISM), Udine, Italy, 1998 (in italian).
[28] T.T. Lie, R.J. Irwin, Evaluation of the Fire Resistance of Reinforced Concrete Columns with Rectangular Cross-Section, National Research Council, Canada, 1990, Internal Report No. 601.
[29] R. Hass, Practical Rules for the Design of Reinforced Concrete and Composite Columns Submitted to Fire, Institut für Baustoffe, Massivbau und Brandschutz der Technischen Universität Braunschweig, 1986, Technical Report No. 69 (in German), Braunschweig, Germany.
[30] J.-C. Dotreppe, J.M. Franssen, A. Bruls, P. Vandevelde, R. Minne, D. Van Nieuwenburg, H. Lambotte, Experimental research on the determination of the main parameters affecting the behavior of reinforced concrete columns under fire condition, Mag. Concr. Res. 49 (179) (1996) 117–127.